Dynamics of the Excited State of Polysilane Dendrimers: Origin of the Broad Visible Emission of Branched Silicon Chains

Akira Watanabe,[†] Masato Nanjo,[‡,§] Tomoyasu Sunaga,[‡] and Akira Sekiguchi*[,‡]

Institute of Multidisciplinary Research for Advanced Materials, Tohoku University, Katahira, Aoba-ku, Sendai 980-8577, Japan, and Department of Chemistry, University of Tsukuba, Tsukuba, Ibaraki 305-8571, Japan

Received: March 5, 2001; In Final Form: April 27, 2001

The excited-state dynamics of polysilane dendrimers are studied using time-resolved emission spectroscopy. The time-resolved emission spectra of polysilane dendrimers showed two bands, one in the UV and one in the visible region. The former was assigned to the emission from the excited state at the linear Si−Si chain, and the latter was assigned to that at the branching points. The intramolecular energy transfer between both excited states was demonstrated by the emission time profile, which showed a growth in intensity with increase in the delay time after laser excitation. The spectral shape of the visible emission can be expressed by a fitted curve using a Gaussian distribution function, which suggests that the configuration coordinates model is applicable to the photophysical processes of a Si−Si chain with a branching point. An MO calculation showed the distorted geometry around the branching point in the excited state, which corresponds to the localized excited state in the configuration coordinates model.

1. Introduction

The emission properties of silicon with a low-dimensional structure is a topic of great interest. In the field of inorganic silicon chemistry, the visible emission from porous silicon has been an exciting research area for the past decade.[1−4] On the other hand, in the field of organosilicon chemistry, polysilanes consisting of a pseudo-one-dimensional silicon main chain and organic side chains have received considerable attention,[5,6] and one of the interests is linked with the emission of inorganic silicon having a low-dimensional structure. Polysilanes with various kinds of silicon skeletons have been reported recently, for example, branched polysilane,[7,8] network polysilane (polysilyne),[9−14] ladder polysilane,[15] silicon nanocluster,[16−21] polysilane dendrimer,[22−29] etc. The visible emission properties of the network polysilanes are characterized by broadness and a large Stokes shift, which are different features from those of linear polysilanes and show a sharp emission in the UV region indicating a mirror image. The red shift of absorption and the emission spectra of network polysilanes, in comparison with linear polysilanes, have been explained by the increase in σ-conjugation along the pseudo-two-dimensional Si−Si chain. The branched polysilane with an intermediate structure between linear and network polysilanes showed two kinds of emission maxima at around 360 and 460 nm.[8] The former is a sharp one and assigned to emission from the linear Si−Si chain. The latter is a broad one that is analogous to that in network polysilane. A similar broad emission is observed for organosilicon nanoclusters, which contain four-coordinated silicon atoms.[19] Such a broad emission in the visible region was also observed for photobleached linear polysilane.[30] The origin of the visible emission was attributed to the presence of defects such as branching points in the linear backbone.[31]

It is clear that the visible broad emission from polysilanes is related to the branching point of the Si−Si chain. However, the assignment of the structure around the branching point is difficult because these polysilanes do not have a regular structure. The inhomogeneity of the Si−Si chain causes the complicated kinetics of the emission processes and analysis of the polydispersed emission kinetics has many difficulties and obscurities. In contrast, a polysilane dendrimer has regular branching Si−Si chains,[22−29] and it is an ideal model for the branched polysilanes. Although one report concerning the emission spectrum of a polysilane dendrimer has appeared, by Suzuki et al.,[24] the dynamics of the excited state are not yet clear. In this paper, we report the excited-state dynamics of the polysilane dendrimer using time-resolved emission spectroscopy and discuss the origin of the visible broad emission. Three kinds of polysilane dendrimers are adopted, as shown in Figure 1. **1G** is a first-generation dendrimer that has four branching points. **2G** is a second-generation dendrimer that has 10 branching points. **0G** corresponds to the basic branching unit of the polysilane dendrimers. In this study, the emissions of the dendrimers were observed in a dilute solution where intermolecular interaction and energy transfer between dendrimer molecules are negligible, because we wished to focus our attention on the intramolecular dynamics of the excited state.

2. Experimental Section

2.1. Materials. Tetrahydrofuran (THF), diethyl ether, hexane, benzene, and toluene were distilled from sodium−benzophenone ketyl, and dichloromethane was distilled from calcium hydride. Methyllithium (LiBr-free diethyl ether solution), trifluoromethanesulfonic acid (TfOH), ammonium chloride, and anhydrous sodium sulfate (Na_2SO_4) were commercially available and were used without further purification. The first- and second-generation polysilane dendrimers **1G** and **2G** were prepared according to the literature.[23,28]

* Author to whom correspondence should be addressed. Fax: +81-298-53-4314. E-mail: sekiguch@staff.chem.tsukuba.ac.jp.

[†] Tohoku University.

[‡] University of Tsukuba.

[§] Present address: Department of Chemistry, Faculty of Science, Gakushuin University, Toshima-ku, Tokyo 171-8588, Japan.

10.1021/jp010840f CCC: $20.00
Published on Web 06/07/2001

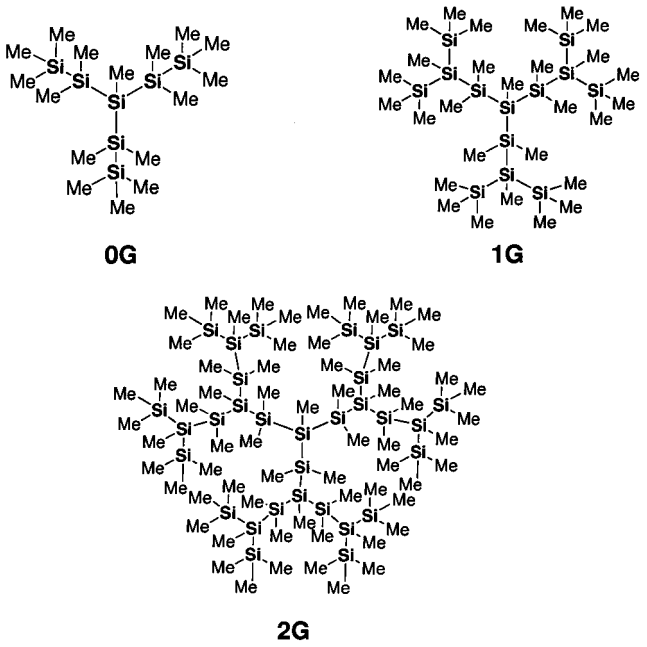

Figure 1. Structural formulas of polysilane dendrimers and the abbreviations.

2.2. 2-Dimethyl(phenyl)silyl-1,1,2,3,3-pentamethyl-1,3-diphenyltrisilane [MeSi(SiMe$_2$Ph)$_3$]. Dimethylphenylsilyllithium (100 mmol) in toluene (50 mL) was added dropwise to methyltrichlorosilane (4.78 g, 32.0 mmol) in hexane (500 mL). The reaction mixture was hydrolyzed with hydrochloric acid followed by extraction with hexane/toluene. The organic layer was washed with water and dried over Na_2SO_4. After evaporation of the solvent, the residual oil was distilled by a Kugelrohr under reduced pressure (ca. 200 °C/0.06 mmHg) to give the title compound (12.46 g, 27.8 mmol) as colorless crystals in 87% yield; ^{1}H NMR ($CDCl_3$, δ) 0.17 (s, 3 H), 0.18 (s, 18 H), 7.25 (brs, 15 H); ^{13}C NMR ($CDCl_3$, δ) −11.7, −1.9, 127.7, 128.3, 133.8, 140.2; ^{29}Si NMR ($CDCl_3$, δ) −86.3, −15.5. Anal. Calcd for $C_{25}H_{36}Si_4$: C, 66.89; H, 8.08. Found: C, 66.94; H, 8.03.

2.3. 1,1,2,2,3,4,4,5,5-Nonamethyl-1,5-diphenyl-3-(1,1,2,2-tetramethyl-2-phenyldisilanyl)pentasilane [MeSi(SiMe$_2$SiMe$_2$Ph)$_3$]. TfOH (0.24 mL, 2.7 mmol) was added to 2-dimethyl(phenyl)silyl-1,1,2,3,3-pentamethyl-1,3-diphenyltrisilane (2.08 g, 4.64 mmol) in dichloromethane (30 mL) at 0 °C. After the mixture was stirred for 1 h, ammonium chloride (2.0 g, 37 mmol) was added to the reaction mixture. The mixture was stirred overnight at room temperature. After removal of excess ammonium chloride by filtration, the solvent was replaced by toluene (20 mL). The solution was treated with dimethylphenylsilyllithium (16 mmol) in toluene (10 mL). After the usual workup, the crude oil was purified by column chromatography on silica gel using a 1:2 toluene/hexane mixture as eluent to give the title compound (1.86 g, 2.97 mmol) as a colorless oil in 64% yield; ^{1}H NMR ($CDCl_3$, δ) 0.03 (s, 18 H), 0.07 (s, 3 H), 0.33 (s, 18 H), 7.27−7.42 (m, 15 H); ^{13}C NMR ($CDCl_3$, δ) −8.6, −2.8, −2.6, 127.7, 128.3, 133.8, 139.7; ^{29}Si NMR ($CDCl_3$, δ) −72.2, −39.9, −17.4. Anal. Calcd for $C_{31}H_{54}Si_7$: C, 59.73; H, 8.73. Found: C, 59.66; H, 8.63.

2.4. 1,1,1,2,2,3,4,4,5,5,5-Undecamethyl-3-(pentamethyldisilanyl)pentasilane [MeSi(SiMe$_2$SiMe$_3$)$_3$] 0G. TfOH (0.25 mL, 2.8 mmol) was added to 1,1,2,2,3,4,4,5,5-nonamethyl-1,5-diphenyl-3-(1,1,2,2-tetramethyl-2-phenyldisilanyl)pentasilane (504 mg, 0.802 mmol) in dichloromethane (10 mL) at 0 °C. After the mixture was stirred for 1 h, ammonium chloride (1.5 g, 28 mmol) was added to the reaction mixture. The mixture was stirred overnight at room temperature. After removal of excess ammonium chloride by filtration, the solvent was replaced by THF (12 mL). The solution was treated with methylmagnesium iodide (21 mmol) in diethyl ether. After the usual workup, the crude oil was purified by column chromatography on silica gel using hexane as an eluent to give the title compound (253 mg, 0.58 mmol) as colorless crystals in 73% yield. Mp 50−51 °C; ^{1}H NMR ($CDCl_3$, δ) 0.09 (s, 27 H), 0.17 (s, 18 H), 0.18 (s, 3 H); ^{13}C NMR ($CDCl_3$, δ) −8.9, −3.0, −0.89; ^{29}Si NMR ($CDCl_3$, δ) −74.2, −40.2, −14.5; MS (*m*/*z* (%)) 436 (M^+, 3), 305 (5), 231 (9), 215 (10), 157 (9), 131 (16), 73 (100). HRMS calcd for $C_{16}H_{48}Si_7$ [M^+] 436.2141, found 436.2140.

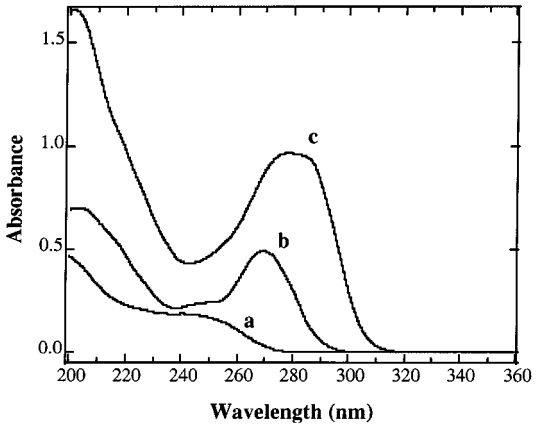

Figure 2. Electronic absorption spectra of **0G** (a), **1G** (b), and **2G** (c) in hexane.

2.5. Measurements. ^{1}H (300 MHz), ^{13}C (75.5 MHz), and ^{29}Si (59.6 MHz) NMR spectra were recorded on a Bruker AC-300 FT spectrometer. Mass spectra were recorded on a Shimadzu GCMS-QP5000 gas-chromatograph mass spectrometer. UV spectra were recorded on a Shimadzu UV-2100 spectrometer. The time-resolved emission spectra were measured using an argon ion laser (Spectra-Physics, BeamLok 2060-10-SA) pumped Ti:sapphire laser (Spectra-Physics, Tsunami 3950-L2S) with a pulse selector (Spectra-Physics, Model 3980), a harmonic generator (GWU-23PS), and a streak scope (HAMAMATSU, C4334−01, sweep repetition rate 2 MHz). In the measurements, by setting a threshold level for the A/D converted CCD camera signal, the photoelectron image can be clearly separated from the noise. The system enables photon counting measurements at simultaneous multiple wavelengths. The typical instrument response time for this apparatus is 20 ps (fwhm) and time resolution of the detection within 5 ps can be obtained by using a deconvolution technique. The polysilane dendrimers were dissolved in 3-methylpentane and the concentration of the sample solutions was controlled below 5×10^{-5} M to reduce intermolecular interaction and energy transfer. The wavelength of the laser excitation is the third harmonic of the Ti:sapphire laser (279 nm). The quantum efficiency of the polysilane dendrimer was determined by using quinine sulfate as a standard. The molecular orbital calculations of a polysilane dendrimer were carried out using the CAChe system (Sony Tektronics). The optimized geometries of the polysilane dendrimer in the ground and excited state were calculated by the PM3 method using the semiempirical MOPAC package.

3. Results and Discussion

3.1. Time-Resolved Emission Spectra of Polysilane Dendrimers. The absorption spectra of polysilane dendrimers in hexane are compared in Figure 2. The absorption maxima of

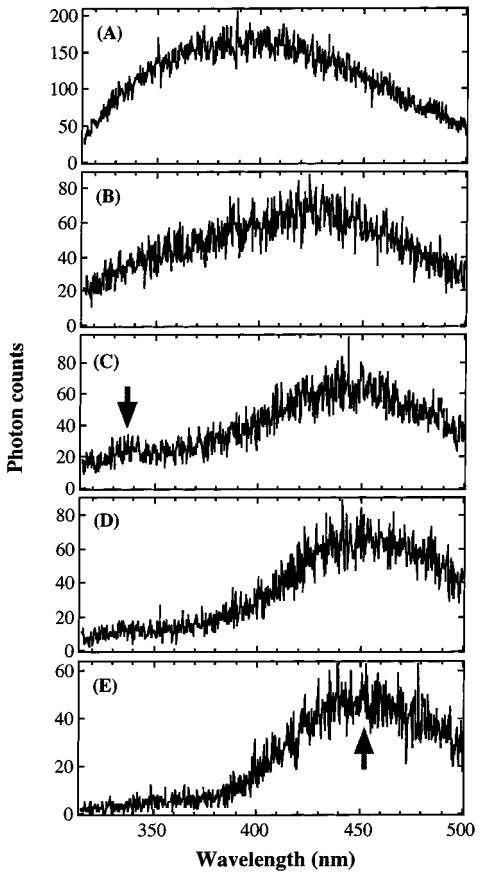

Figure 3. Time-resolved emission spectra of **0G** in 3-methylpentane at 77 K: (A) 0−5 ns, (B) 5−10 ns, (C) 10−20 ns, (D) 20−40 ns, (E) 40−60 ns. Excitation wavelength: 279 nm.

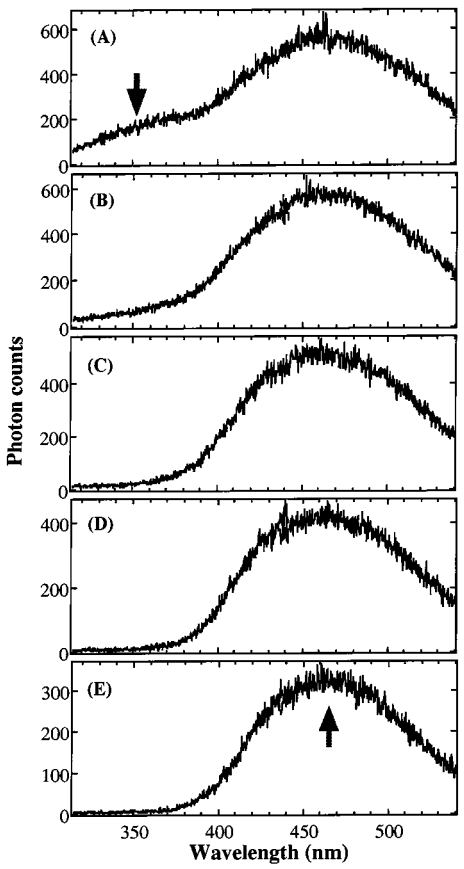

Figure 4. Time-resolved emission spectra of **1G** in 3-methylpentane at 77 K: (A) 0−2 ns, (B) 2−4 ns, (C) 5−7 ns, (D) 10−12 ns, (E) 20−22 ns. Excitation wavelength: 279 nm.

0G, **1G**, and **2G** are 242, 269, and 279 nm, respectively. With increase in the size of the Si−Si chain, the absorption spectrum shows a red shift, which is attributed to the enhancement of σ-conjugation along the Si−Si chain. The longest linear sequence of Si atoms for **2G** is 11 while those for **0G** and **1G** are 5 and 7, respectively. Thermochromism of the polysilane dendrimer was not observed because of the rigidity of the Si−Si chain of the dendrimer compared with the linear polysilane.

The time-resolved emission spectra for **0G** in a rigid 3-methylpentane matrix at 77 K are shown in Figure 3. The remarkable feature in Figure 3 is the spectral change upon increasing the delay time after laser excitation. At the early stage within 40 ns, UV emission around 340 nm is observed, which is indicated by the arrow in Figure 3C. This UV emission can be attributed to that from a linear part of the Si−Si chain. On increasing the delay time, the relative intensity of the UV emission decreases in comparison with a broad emission in the visible region around 450 nm. The spectral shape of the visible emission quite resembles the emission spectra of the branched polysilanes. The dendrimer **1G** also shows a similar spectral change, as shown in Figure 4, however, the emission maxima of the UV and visible emissions are shifted to 350 and 460 nm, respectively. The red shifts correspond to the shift of the absorption spectrum, as shown in Figure 2.

There are two possibilities to explain the two emission bands in the UV and visible regions. The first is that the dendrimer has two kinds of emissive points, such as linear and branching parts of the Si−Si chain. Another is the effect of an impurity, that is, the sample solution contains two compounds. The latter can be rejected by investigating the time-profiles of the UV and visible emissions as follows: Figure 5 shows the logarithmic

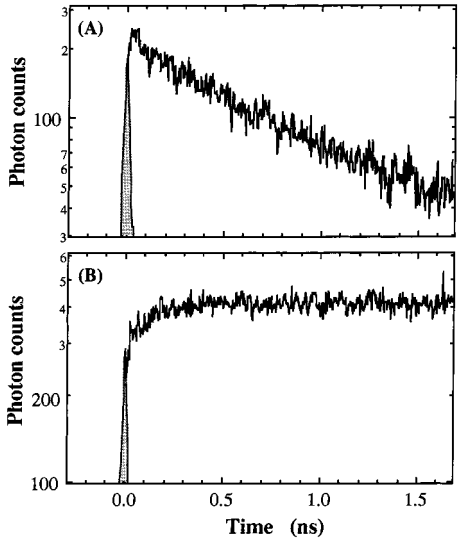

Figure 5. Logarithmic plot of the time-profile for the emission of **1G** in 3-methylpentane at 77 K: (A) time-profile monitored at 350 nm; (B) time-profile monitored at 460 nm.

plot of the time-profile for the emission of **1G** in 3-methylpentane at 77 K monitored at 350 and 460 nm. The logarithmic plot for the emission decay of **1G** monitored at 350 nm shows a straight line, which suggests a single-exponential decay of the emission. The single-exponential decay curve is reasonable behavior for an isolated molecule located in a dilute solution. On the other hand, the logarithmic plot for the time-profile monitored at 460 nm shows the gradual growth of the emission intensity upon increasing the delay time. The growth is

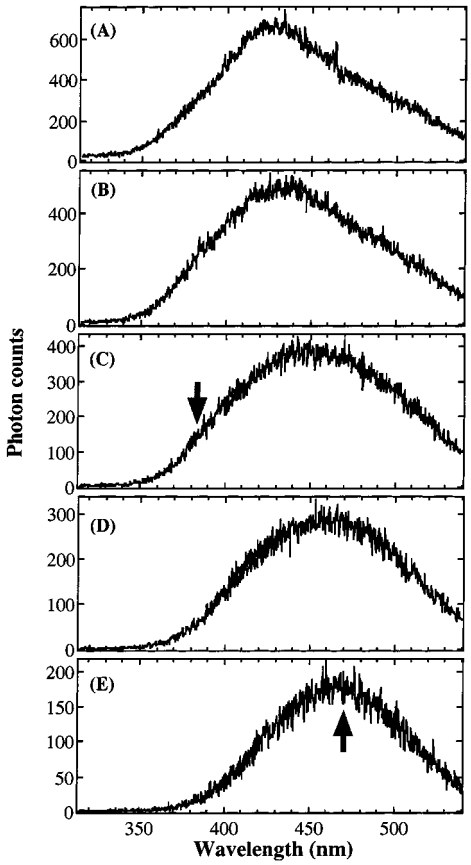

Figure 6. Time-resolved emission spectra of **2G** in 3-methylpentane at 77 K: (A) 0−2 ns, (B) 2−4 ns, (C) 5−7 ns, (D) 10−12 ns, (E) 20−22 ns. Excitation wavelength: 279 nm.

attributable to intramolecular energy transfer (energy migration) because the concentration of the sample solution is below 5×10^{-5} M and so is dilute enough to inhibit intermolecular energy transfer. These results suggest that the polysilane dendrimer has two kinds of emissive structures, and that the excited state is transferred from the UV-emissive structure to the visible-emissive one, which can be attributed to the linear and branching points of the dendrimer Si−Si chain. It is surprising that the two emission bands in the UV and visible regions were observed even for the small **0G** unit. This may be due to the small energy gap between the two kinds of excited states and random hopping between them. The energy gap will be estimated in a later section by observing the temperature dependence of the lifetimes.

Figure 6 shows the time-resolved emission spectra of **2G** in 3-methylpentane at 77 K. In the case of **2G**, the broad visible emission is the main band and the UV emission band is not apparent. The emission shoulder around 380 nm must be assigned to the emission from the linear Si−Si chain. As shown in Figure 7, the broad visible emission band can be fitted by using a Gaussian distribution curve. The large Stokes shift of the emission band and the spectral shape expressed by the Gaussian distribution curve are characteristics of the excited state explained by the configuration coordinates model. In Figure 8, the excited state of the polysilane dendrimer is illustrated by using the configuration coordinates model. The large Stokes shift is explained by the different minimum energy points along the configuration coordinates. After photoexcitation, a localized excited state is generated by distortion of the molecules in the excited state. The population of the energy levels on the potential curve in the excited state can be expressed by the Gaussian

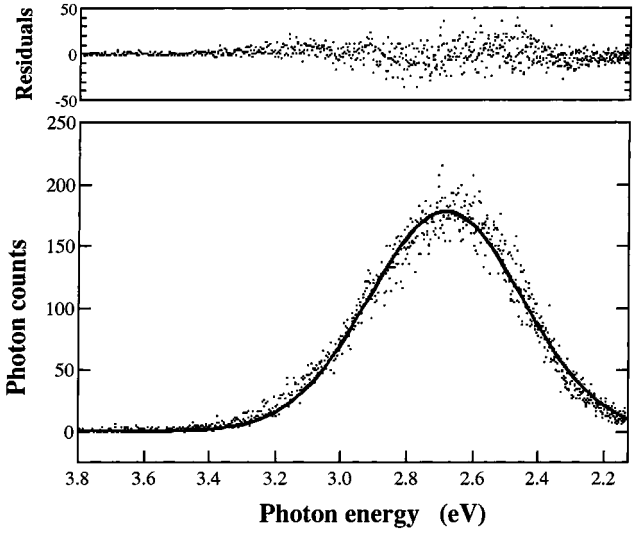

Figure 7. Emission spectrum of **2G** at 20−22 ns and the fitting curve using Gaussian function.

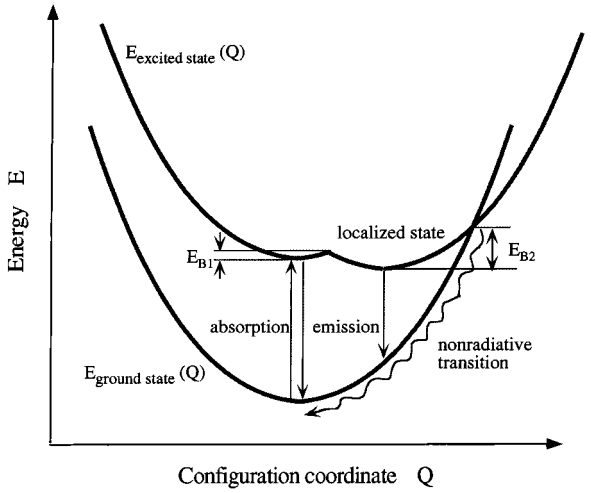

Figure 8. Configuration coordinates model for polysilane dendrimer.

distribution curve. The broadness of the emission spectrum is caused by the thermal distribution of the energy levels in the excited state and the transition to the curvature of the potential curves in the ground state. In the case of the polysilane dendrimer, the emission in the UV and visible regions suggests the existence of two kinds of excited states on the potential curve. Another feature of the configuration coordinates model is deactivation of the excited state via the crossing point between potential curves for the ground and excited states. The nonradiative transition reduces the emission quantum efficiency. In fact, the quantum efficiency of the broad visible emission of a network polysilane is 0.001 while the linear polysilane with a small Stokes shift shows a quantum efficiency higher than 0.1.[31] The quantum efficiency of the polysilane dendrimer is also not very high, that of **1G** was determined to be 0.014, which is due to the nonradiative transition as depicted in Figure 8. The energy barrier E_B for the nonradiative transition is determined in a later section from the temperature dependence of the emission lifetime.

3.2. Wavelength Dependence of the Emission Lifetime. As shown in Figures 3, 4, and 6, the emission spectra show a red shift upon increasing the delay time after laser excitation. In the case of **2G**, the emission maximum at 425 nm gradually shifts to 470 nm just after the laser excitation upon increasing the delay time to 20 ns. The analysis of the wavelength

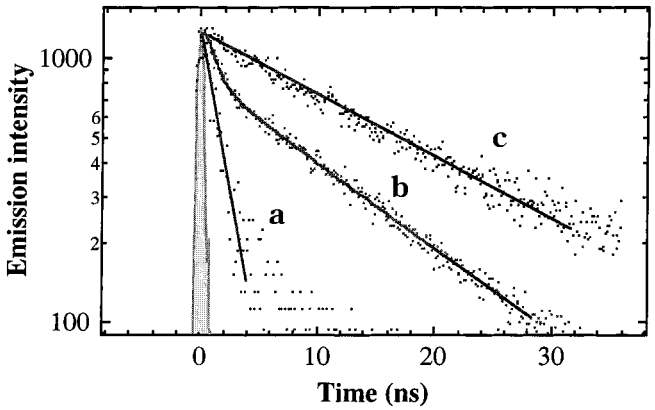

Figure 9. Logarithmic plot of the time-profile for the emission of **2G** in 3-methylpentane at 77 K and the fitting curves using two exponential equation: (a) 325 nm, (b) 425 nm, (c) 515 nm.

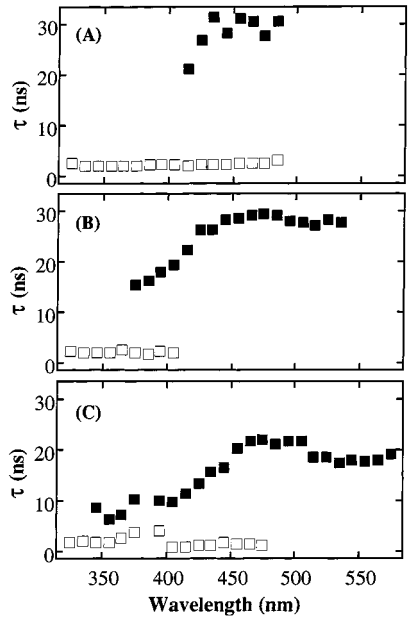

Figure 10. Wavelength dependence of lifetimes of **0G** (A), **1G** (B), and **2G** (C).

dependence of the lifetime is effective in determining what kinds of components are involved in the emission spectrum. The wavelength dependence of the emission decay curves is depicted in Figure 9 for **2G** in 3-methylpentane at 77 K monitoring at 325, 425, and 515 nm. The decay curves monitored at 325 and 515 nm, which correspond to the UV and visible emission, respectively, obey first-order kinetics. On the other hand, the decay at 425 nm is not a single-exponential decay curve. The decay curve was well fitted by using the equation consisting of two exponential functions, $I(t) = A \exp(-t/\tau_1) + B \exp(-t/\tau_2)$, where $I(t)$ is the emission intensity at the delay time t, τ_1 is the shorter lifetime, and τ_2 is the longer lifetime. The fitted curve is depicted by the solid curve in Figure 9.

By using the two-exponential equation, the lifetimes τ_1 and τ_2 were determined for **0G**, **1G,** and **2G** at various wavelengths. The lifetimes are plotted against the monitoring wavelengths in Figure 10. In the case of **0G**, as shown in Figure 10A, the decay curves at wavelengths below 405 nm obey the single-exponential equation and the lifetimes are determined to be 2.11 $\pm$ 0.26 ns. At wavelengths longer than 415 nm, the emission decay curves did not obey the single-exponential equation and the two-exponential equation was applied to determine the shorter lifetime τ_1 and the longer lifetime τ_2, which correspond to the lifetimes of the UV and visible emissions, respectively. In the region from 435 to 485 nm, the lifetimes τ_1 and τ_2 are almost constant and determined to be 2.63 $\pm$ 0.6 and 30.0 $\pm$ 2 ns, respectively. In the intermediate region between 415 and 435 nm, significant changes of τ_2 from 21.1 to 31.5 ns were observed. Such a transient behavior in the intermediate region between the UV and visible emission bands becomes more remarkable upon increasing the size of the Si−Si chain as shown in the lifetime plots of **1G** and **2G**. In the case of **1G**, the emission decay curves below 365 nm and above 415 nm are single exponential and the lifetimes τ_1 and τ_2 were determined to be 2.19 $\pm$ 0.2 and 27.5 $\pm$ 5 ns, respectively. In the intermediate region from 375 to 405 nm, although the shorter lifetime τ_1 is almost constant (1.95 $\pm$ 0.3 ns), the longer lifetime τ_2 increases from 15.4 to 19.3 ns, as shown in Figure 10B. In the case of **2G**, the region of single-exponential decay for τ_1 is limited between 325 and 335 nm, where the average lifetime τ_1 is 1.88 ns. Nonexponential decays are observed in a wide region between 345 and 475 nm, as shown in Figure 10C. In the region between 345 and 475 nm, the longer lifetime τ_2 increases from 8.53 (345 nm) to 21.9 ns (475 nm) while the shorter lifetime τ_1 is almost constant, the average lifetime τ_1 is 1.78 ns. In the region above 485 nm, the decay curves obey the single-exponential equation and the lifetime τ_2 was determined to be 19.2 $\pm$ 3 ns.

The lifetime τ_2 in the intermediate region where significant wavelength dependence was observed may be attributed to the excited state, which does not have a fully relaxed conformation in the rigid 3-methylpentane matrix at 77 K after photoexcitation. The large Stokes shift of the visible emission suggests a change of the Si−Si chain geometry in the excited state. Such a geometrical change of the Si−Si chain occurs freely in a fluid solution. However, in the rigid 3-methylpentane matrix, the conformational distribution of the Si−Si chain is fixed, and a geometrical change after photoexcitation is hindered. It is well-known that σ-conjugation of polysilane is quite sensitive to the conformation of the Si−Si chain.[5] The emission in the intermediate region must be assigned to emission from the excited state that has an intermediate geometry between those for the UV and visible emissions. Because of the distribution of geometries in the excited state, continuous changes of the lifetime τ_2 are observed in the intermediate region, as shown in Figure 10. Such distortion of the geometry in the excited state is characteristic of σ-conjugated compounds consisting of Si−Si chains.

The geometrical distortion of the Si−Si chain in the excited state was estimated by semiempirical MO calculations for the ground and excited states. Figure 11 shows the conformations of **0G** in the ground and excited states by semiempirical MO calculations using the PM3 method, where the geometries of Si and C atoms except H are depicted. The initial geometry was constructed based on the crystalline structure of the polysilane dendrimer, and then the conformation was optimized by the MO calculation. In comparison with conformation A in the ground state, conformation B in the excited state shows changes of the bond angles. The remarkable feature of conformation B in the excited state is the unusual bond angle of 60° for the Si(1)−Si(4)−Si(5) sequence. Overlap of the electron cloud and an interaction between Si(1) and Si(5) were suggested by the MO calculation in the excited state. The bond order between Si(1) and Si(5) increased from 0.005 in the ground state to 0.047 in the excited state. Therefore, the Si(1), Si(4), and Si(5) atoms form a structure similar to the Si three-membered ring in the excited state. The visible emission can

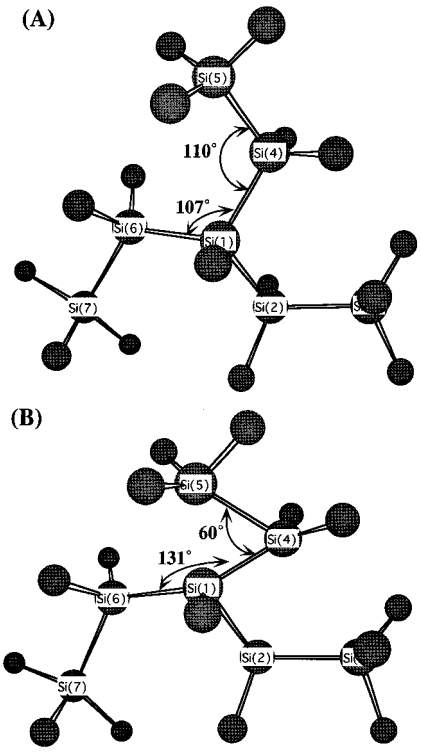

Figure 11. Conformations of ground and excited states of **0G** by semiempirical MO calculations using PM3 method: (A) ground state, (B) excited state.

be attributed to that from the localized excited state that is induced by the distortion of the Si−Si chain around the branching point in the excited state. On the other hand, the MO calculations for a linear Si−Si chain did not show such a serious distortion in the excited state. In the case of a homogeneous Si−Si chain of the linear polysilane, the extension of the σ-electron cloud along the linear Si−Si chain works as a buffer for the distortion, which is induced by the difference of the electron distribution between the ground and excited states. In contrast to this, in the case of the branched polysilane, the distortion is focused on the branching points, and the σ-conjugation is discontinued at those points, forming the localized excited-state having a triangle structure as shown in Figure 11B. The behavior is analogous to that of a self-trapped exciton. In Figure 11B, the increase of the bond angle for the Si(6)−Si(1)−Si(4) sequence must be caused by steric hindrance of the Si(6) atom and the methyl groups.

3.3. Temperature Dependence of the Emission Lifetime. Figure 12 shows the temperature dependence of the lifetimes for the UV and visible emission for **1G** and **2G**. The monitoring wavelengths are limited to those where single-exponential decay curves are observed. The temperature dependence of the emission decay from the localized excited-state expressed by the configuration coordinates model obeys the following equation: $\tau^{-1} = \tau(0\ \mathrm{K})^{-1} + \nu \exp(-E_B/k_BT)$, where E_B, ν, and k_B are energy barrier, frequency factor, and Boltzmann constant, respectively. The energy barrier, E_B, concerns the barrier for the nonradiative deactivation, as shown in the illustration of the configuration coordinates model (Figure 8). In Figure 12, the solid and broken curves are fitted curves based on the above equation. From the curve fittings, the energy barriers E_{B1} and E_{B2} from the temperature dependence of τ_1 and τ_2 for **1G** are determined to be 0.92 and 3.17 kcal/mol, respectively. E_{B1} corresponds to the energy barrier for the energy transfer from the UV-emissive structure to the visible-emissive one, which

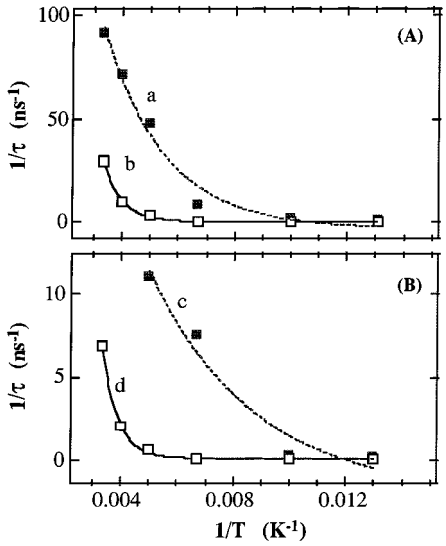

Figure 12. Temperature dependence of lifetimes of **1G** (A) and **2G** (B) in 3-methylpentane and the fitting curves: (a) 345 nm, (b) 460 nm, (c) 380 nm, (d) 470 nm.

can be attributed to the linear chain and branching points of the dendrimer Si−Si chain. The small energy barrier suggests that the excited state at the linear Si−Si chain is easily transferred to the branching point. However, the observation of UV emission even for **0G** also suggests that the branching points work as a shallow trapping site and that detrapping from the branching point is easy. E_{B2}, from the temperature dependence of τ_2, corresponds to the energy barrier for the nonradiative deactivation of the excited state around the branching point. The low quantum efficiency of **1G** ($\Phi = 0.014$) is explained by the low energy barrier. For **2G**, the energy barriers E_{B1} and E_{B2} are determined to be 0.53 and 3.56 kcal/mol, respectively. The E_{B2} values were comparable between **1G** and **2G**. The decrease of UV emission on increasing the dendrimer size may be explained by the smaller E_{B1} value of **2G** in comparison with that of **1G**, which suggests that the efficiency of energy migration is enhanced on increasing the trapping site around the UV emissive excited state.

4. Conclusion

Time-resolved emission spectra of polysilane dendrimers showed the two bands in the UV and visible regions. The former was assigned to the emission from the excited state at the linear Si−Si chain, and the latter was assigned to that at the branching points. Intramolecular energy transfer between both excited states was demonstrated by the emission time-profile, which showed a growth in the emission intensity upon increasing the delay time after laser excitation. The spectral shape of the visible emission can be expressed by a fitted curve using the Gaussian distribution function, which suggests that the configuration coordinates model is applicable to emission from the Si−Si chain with a branching point. The energy barriers for energy transfer and nonradiative deactivation were determined from the temperature dependence of the emission lifetime. The wavelength dependence of the lifetime of the visible emission suggested the distribution of the Si chain conformation in the rigid 3-methylpentane matrix at 77 K. The MO calculation showed the distorted geometry around the branching point in the excited state, which corresponds to the localized excited state in the configuration coordinates model.

Acknowledgment. This work was supported by Grants-in-Aid for Scientific Research (Nos. 12042213, 13029015, 13440185, 11559003, 11650917) from the Ministry of Education, Science and Culture of Japan, and TARA (Tsukuba Advanced Research Alliance) fund.

References and Notes

(1) Canham, L. T. *Appl. Phys. Lett.* **1990**, *57*, 1046.
(2) Heinrich, J. L.; Curtis, C. L.; Gredo, G. M.; Kavanagh, K. L.; Sailor, M. J. *Science* **1992**, *255*, 66.
(3) Vial, J. C.; Derrien, J. *Porous Silicon Science and Technology*; Springer-Verlag: Berlin, 1995.
(4) Kamimura, H.; Kanemitsu, Y.; Kondo, M.; Takeda, K. *Light Emission from Novel Silicon Materials*; The Physical Society of Japan: Tokyo, 1994.
(5) Miller, R. D.; Michl, J. *Chem. Rev.* **1989**, *89*, 1359.
(6) Trefonas, P., III; Damewood, J. R., Jr.; West, R.; Miller, R. D. *Organometallics* **1985**, *4*, 1318.
(7) Wilson, W. L.; Weidman, T. W. *J. Phys. Chem.* **1991**, *95*, 4568.
(8) Watanabe, A.; Miike, H.; Tsutsumi, Y.; Matsuda, M. *Macromolecules* **1993**, *26*, 2111.
(9) Bianconi, P. A.; Weidman, T. W. *J. Am. Chem. Soc.* **1988**, *110*, 2342.
(10) Bianconi, P. A.; Schilling, F. C.; Weidman, T. W. *Macromolecules* **1989**, *22*, 1697.
(11) Furukawa, K.; Fujino, M.; Matsumoto, N. *Macromolecules* **1990**, *23*, 3423.
(12) Watanabe, A.; Matsuda, M. *Chem. Lett.* **1991**, 1101.
(13) Watanabe, A.; Matsuda, M.; Yoshida, Y.; Tagawa, S. *ACS Symp. Ser.* **1994**, *579*, 408.
(14) Brus, L. *J. Phys. Chem.* **1994**, *98*, 3575.
(15) Matsumoto, H.; Miyamoto, H.; Kojima, N.; Nagai, Y. *J. Chem. Soc., Chem. Commun.* **1987**, 1316.
(16) Heath, J. R. *Science* **1992**, *258*, 1131.
(17) Bley, R. A.; Kauzlarich, S. M. *J. Am. Chem. Soc.* **1996**, *118*, 12461.
(18) Watanabe, A.; Fujitsuka, M.; Ito, O.; Miwa, T. *Jpn. J. Appl. Phys.* **1997**, *36*, L1265.
(19) Watanabe, A.; Fujitsuka, M.; Ito, O.; Miwa, T. *Mol. Cryst. Liq. Cryst.* **1998**, *316*, 363.
(20) Watanabe, A.; Fujitsuka, M.; Ito, O. *Thin Solid Film* **1999**, *354*, 13.
(21) Yang, C.-S.; Bley, R. A.; Kauzlarich, S. M.; Lee, H. W. H.; Delgado, G. R. *J. Am. Chem. Soc.* **1999**, *121*, 5191.
(22) Lambert, J. B.; Pflug, J. L.; Stern, C. L. *Angew. Chem., Int. Ed. Engl.* **1995**, *34*, 98.
(23) Sekiguchi, A.; Nanjo, M.; Kabuto, C.; Sakurai, H. *J. Am. Chem. Soc.* **1995**, *117*, 4195.
(24) Suzuki, H.; Kimata, Y.; Satoh, S.; Kuriyama, A. *Chem. Lett.* **1995**, 293.
(25) Lambert, J. B.; Pflug, J. L.; Denari, J. M. *Organometallics* **1996**, *15*, 615.
(26) Lambert, J. B.; Pflug, J. L.; Stern, C. L. *Organometallics* **1998**, *17*, 4904.
(27) Nanjo, M.; Sekiguchi, A. *Organometallics* **1998**, *17*, 492.
(28) Nanjo, M.; Sunaga, T.; Sekiguchi, A.; Horn, E. *Inorg. Chem. Commun.* **1999**, *2*, 203.
(29) Sekiguchi, A.; Lee, V. Ya.; Nanjo, M. *Coord. Chem. Rev.* **2000**, *210*, 11.
(30) Watanabe, A.; Tsutsumi, Y.; Matsuda, M. *Synth. Met.* **1995**, *74*, 191.
(31) Fujiki, M. *Chem. Phys. Lett.* **1992**, *198*, 177.